Available online at www.sciencedirect.com

SCIENCE DIRECT®

Journal of Volcanology and Geothermal Research 135 (2004) 127–146

Journal of volcanology and geothermal research

www.elsevier.com/locate/jvolgeores

Spaceborne observations of the 2000 Bezymianny, Kamchatka eruption: the integration of high-resolution ASTER data into near real-time monitoring using AVHRR

Michael Ramsey[a,*], Jonathan Dehn[b]

[a] *Department of Geology and Planetary Science, University of Pittsburgh, 200 SRCC Building, Pittsburgh, PA 15260, USA*
[b] *Geophysical Institute/Alaska Volcano Observatory, University of Alaska, Fairbanks, AK 99775, USA*

Accepted 5 December 2003

Abstract

Since its launch in December 1999, the Advanced Spaceborne Thermal Emission and Reflection Radiometer (ASTER) instrument has been observing over 1300 of the world's volcanoes during the day and night and at different times of the year. At the onset of an eruption, the temporal frequency of these regularly scheduled observations can be increased to as little as 1–3 days at higher latitudes. However, even this repeat time is not sufficient for near real-time monitoring, which is on the order of minutes to hours using poorer spatial resolution (>1 km/pixel) instruments. The eruption of Bezymianny Volcano (Kamchatkan Peninsula, Russia) in March 2000 was detected by the Alaska Volcano Observatory (AVO) and also initiated an increased observation frequency for ASTER. A complete framework of the eruptive cycle from April 2000 to January 2001 was established, with the Advanced Very High Resolution Radiometer (AVHRR) data used to monitor the large eruptions and produce the average yearly background state for the volcano. Twenty, nearly cloud-free ASTER scenes (2 days and 18 nights) show large thermal anomalies covering tens to hundreds of pixels and reveal both the actively erupting and restive (background) state of the volcano. ASTER short-wave infrared (SWIR) and thermal infrared (TIR) data were also used to validate the recovered kinetic temperatures from the larger AVHRR pixels, as well as map the volcanic products and monitor the thermal features on the summit dome and surrounding small pyroclastic flows. These anomalies increase to greater than 90 °C prior to a larger eruption sequence in October 2000. In addition, ASTER has the first multispectral spaceborne TIR capability, which allowed for the modeling of micrometer-scale surface roughness (vesicularity) on the active lava dome. Where coupled with ongoing operational monitoring programs like those at AVO, ASTER data become extremely useful in discrimination of small surface targets in addition to providing enhanced volcanic mapping capabilities.

Keywords: Bezymianny Volcano; ASTER; AVHRR; eruption; Alaska Volcano Observatory (AVO)

1. Introduction

With the new series of satellite instruments now orbiting the Earth, never before available data with higher resolutions and design features are now being used for volcanic studies. In 1991, the National Aero-

* Corresponding author. Tel.: +1-412-624-8772; fax: +1-412-624-3914.
E-mail address: ramsey@ivis.eps.pitt.edu (M. Ramsey).

0377-0273/$ - see front matter © 2004 Elsevier B.V. All rights reserved.
doi:10.1016/j.jvolgeores.2003.12.014

nautic and Space Administration (NASA) launched a comprehensive program to study the Earth as one environmental system, now called the Earth Science Enterprise (Kaufman et al., 1999). The program began with several single-instrument satellites and continued in early 1999 with the launch of Landsat 7 containing the Enhanced Thematic Mapper Plus (ETM+) instrument. *Terra*, the first Earth Observing System (EOS) satellite, was launched later that year and has five instruments focused on land and atmospheric processes. The second, *Aqua*, was successfully launched in May 2002 and is focusing observations on the hydrologic cycle. The EOS satellite instruments have entered a planned long-term global monitoring phase, providing integrated measurements on the interactions between the Earth's global cycles. Included in this effort are the science investigations that examine the solid Earth cycle, including the associated natural hazards such as volcanic eruptions.

Remote sensing of active volcanoes has taken place for decades providing critical monitoring information on the state of unrest and the potential of future hazards for many volcanoes throughout the world (Kieffer et al., 1981; Glaze et al., 1989; Harris et al., 2001; Flynn et al., 2002; Dean et al., 2002a,b). Satellite instruments such as the Total Ozone Mapping Spectrometer (TOMS), the Moderate-Resolution Imaging Spectroradiometer (MODIS), and the Geostationary Operational Environmental Satellite (GOES) each have been used for monitoring and to decipher fundamental volcanic questions pertaining to processes operating at the edifice and within the volcanic plume (Oppenheimer, 1993; Realmuto et al., 1994; Wooster and Kaneko, 1998; Harris et al., 1998, 1999; Schneider et al., 1999). In order to provide this operational near real-time monitoring, high (minutes–hours) temporal frequency data are required (Harris et al., 1999; Dehn et al., 2000). However, such systems cannot provide the necessary spectral or spatial resolution in order to perform more detailed observations at the scale of the lava flow or dome. Such data are important as they are sensitive to smaller scales, which can reveal subtle eruptive precursor activity and be used for modeling surface changes.

The work presented here describes the initial phase of a study fusing the high spatial, moderate spectral resolution Advanced Spaceborne Thermal Emission and Reflectance Radiometer (ASTER) data with the low spatial, low spectral resolution Advanced Very High Resolution Radiometer (AVHRR) data over the active dome complex of Bezymianny Volcano. It serves to calibrate and validate the plan to integrate data like ASTER into an operational, near real-time monitoring system used by the Alaska Volcano Observatory (Ramsey and Dehn, 2002). Such a system would rely on the detection frequency of AVHRR to virtually trigger an ASTER acquisition in order to examine the volcanic surface and plume in detail. However, this study also resulted in a comparative analysis between the two sensors and produced a time series of changes in the volume, morphology, temperature distribution, and surface vesicularity for the Bezymianny dome.

2. Instrument background and comparison

2.1. AVHRR

The volcanoes of the northern Pacific region pose a serious threat not only to the sparse local population, but to the air traffic in the region (Miller and Casadevall, 2000). The primary mission of AVO is therefore to mitigate the hazard to air traffic, by monitoring the volcanoes through conventional geophysical techniques such as seismic and global positioning system (GPS) as well as remote sensing. Most of the volcanoes in the region are remote and cannot be observed easily or cheaply, and therefore satellite images (primarily AVHRR) provide the only reliable means for monitoring. For example, the hazards resulting from the 2001 eruption of Mt. Cleveland volcano were entirely mitigated using satellite data (Dean et al., 2002a,b). Because no geophysical instrumentation was present on the island, AVHRR data were acquired, analyzed and the results communicated to all interested parties, thereby avoiding any loss of life and property.

The AVHRR sensor is the primary device on the National Oceanographic and Atmospheric Administration's (NOAA) polar orbiting weather satellites, having a nadir resolution of 1.1 km in five bands covering the visible to thermal infrared (Table 1). It forms the backbone of AVO's satellite monitoring for the 150 potentially active volcanoes in this region

Table 1
AVHRR instrument specifications

	VNIR	SWIR	TIR
Wavelength range (μm)	0.58–1.1	3.55–3.93	10.3–12.5
Number of channels	2	1	2
Spatial resolution	1.1 km	1.1 km	1.1 km
Nominal repeat time	4–6 h	4–6 h	4–6 h
View angle	± 53°	± 53°	± 53°

(Dean et al., 1998, 2002b). These data have been available, tested, and archived for the past 10 years, making AVHRR the most reliable, long-term data set available on the thermal character of the Kurile–Kamchatkan–Aleutian Arc volcanoes. At these high latitudes up to 12 passes are received each day for the Cook Inlet volcanoes, decreasing to only 1–2 for volcanoes at the edge of the AVO station mask (Fig. 1). Therefore, the best use of this images is to detect thermal changes over days to weeks.

The AVHRR data are automatically processed and distributed to analysts through the Internet, and on internal image processing systems (Dean et al., 2002a,b). In addition to twice-daily inspection of the data, AVO has developed several automated monitoring techniques to alert staff in the event of a volcanic eruption. One such technique, dubbed the Okmok Algorithm was named for the volcano where it was first used. It scans AVHRR data for a region around the volcano, picks out the warmest band 3 (3.5–3.9 μm) pixel and stores both the time and temperature values. Over time, these values form a background state for each volcano. When a volcano suddenly rises above that background state, an electronic mail alert is sent to an AVO analyst (Dehn et al., 2000). All automated detection of volcanic activity is inspected by an analyst before a formal eruption alert is issued to state and federal agencies.

In addition to AVHRR data, other satellite systems are also utilized including GOES as well as the MODIS instrument on both the *Terra* and *Aqua* satellites (Flynn et al., 2002). Higher spatial resolution images of opportunity are also obtained during increased activity at a given volcano, including Landsat ETM+, Ikonos, and synthetic aperture radar (SAR).

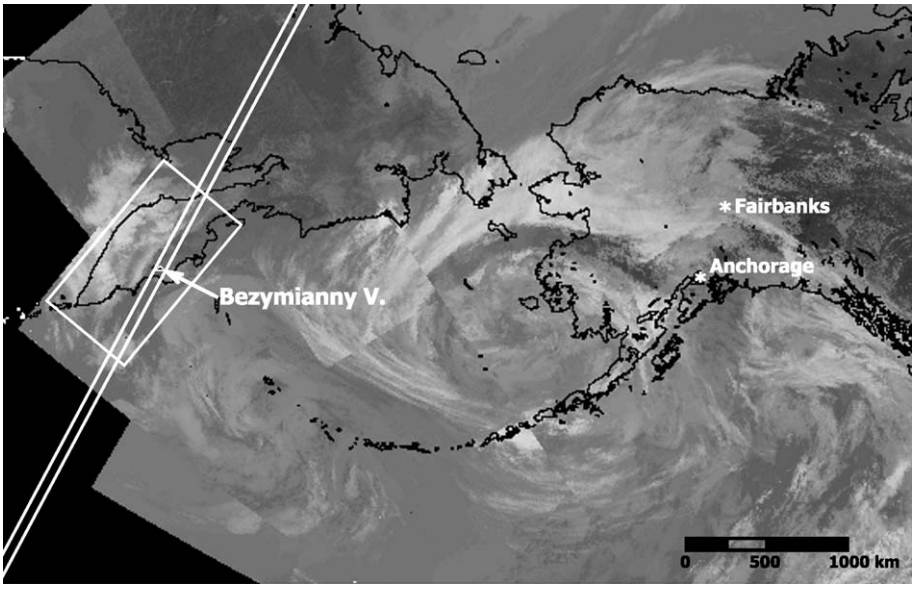

Fig. 1. AVHRR satellite composite over the northern Pacific Ocean, defining the western-most maximum extent of the AVO station mask. This composite of 10 thermal infrared images acquired on 8 June 1998 shows typical meteorological clouds in white and an obvious polar low-pressure system north of the Aleutian Islands. Also shown are the approximate location of one ASTER ascending (night time) orbit track over the Kamchatkan Peninsula, the location of Bezymianny Volcano (arrow and white triangle), as well as the area covered by Fig. 2 (white rectangle).

Each of these has specific uses to detect activity or evaluate various conditions of a volcano; however, none is collected in a formalized way as part of the automated eruption monitoring and alert system. This work represents the first step in a plan to integrate such opportunistic data (ASTER) into an operational volcano monitoring system (Ramsey and Dehn, 2002).

2.2. ASTER

ASTER was one of five sensors launched on the *Terra* satellite in December 1999 as part of the NASA Earth Observing System. The Terra platform follows a Sun-synchronous, nearly polar orbit slightly more than 30 min behind the Landsat 7 satellite, which results in a nominal repeat time of 16 days for the instrument (Table 2). ASTER initiated its nominal calibrated data release in November 2000, although initial calibration data now exist back to early March 2000. It was designed to acquire repetitive, high spatial resolution, multispectral data over the visible/near infrared (VNIR), the short-wave infrared (SWIR) and the thermal infrared (TIR) portions of the spectrum (Kahle et al., 1991; Yamaguchi et al., 1998; Abrams, 2000; Pieri and Abrams, 2004). In order to accomplish that task, ASTER is comprised of three separate subsystems operating with three channels in the VNIR, six channels in the SWIR and five channels in the TIR (Table 2). The spatial resolution decreases from 90 to 30 to 15 m in the TIR, SWIR and VNIR, respectively.

ASTER has numerous unique design features making it far superior to the Landsat TM class of instruments. In particular for volcanic observations, five main features are very important. First, and perhaps the most critical, is the strategy of routine night time acquisition of SWIR and TIR data for all high-temperature targets. This allows far more data to be collected at any active volcano and eliminates the reduced data acquisitions that occur for ETM+ during the high-latitude winter months. Second, ASTER has a cross-track pointing capability of up to 24° off nadir (~ 320 km), allowing an increased temporal frequency for any target as well as image collection up to ± 85° latitude. Third, the instrument can generate along-track digital elevation models (DEMs) by way of one backward-looking telescope in the near IR. The resulting DEMs can be processed to a resolution of 15 m using the parallax between the two images (Welch et al., 1998). Fourth, ASTER data are acquired using one of several pre-scheduled dynamic ranges in order to mitigate data saturation over highly reflective targets (i.e., snow/ice) and over low signal to noise (minimally reflective) targets (i.e., water). And finally, ASTER provides more than two bands in the TIR for the first time from space. This allows the extraction of emissivity spectra, which can be deconvolved to retrieve the compositional and textural properties of the surface. All of these unique properties are providing new tools with which to monitor and model the small-scale variability of volcanic activity, such as changes in dome morphology, volume, composition, and temperature.

Table 2
ASTER instrument specifications

	VNIR	SWIR	TIR
Wavelength range (μm)	0.52–0.86	1.60–2.43	8.13–11.65
Number of channels	3 (plus 1 back-looking)	6	5
Spatial resolution	15 m	30 m	90 m
Nominal repeat time	5 days	16 days	16 days
Pointing angle	± 24°	± 8.55°	± 8.55°

In addition to the aforementioned features, ASTER also differs from the Landsat TM class of instruments in the way it acquires data. Due to the large data volume generated, the onboard storage capacity and the time needed for cooling of the SWIR and TIR detector assemblies, it operates on an average 8% duty cycle per orbit (16% for the TIR). This limited acquisition time coupled with the adjustable pointing and gain settings requires daily scheduling of the instrument prior to each orbit. This schedule contains the instrument pointing angle, sensors, gain settings and numerous other parameters for each observed target. It can be modified up to the time of upload if, for example, an emergency arises.

The ASTER science team has put into place a series of dedicated global data acquisitions designated as Science Team Acquisition Requests (STARs), which comprise 25% of the total resource allocation of ASTER (Yamaguchi et al., 1998). Each is designed

to ensure the collection of large data sets including the Global Land Ice Measurements from Space (GLIMS) STAR (Raup et al., 2000; Bishop et al., 2000), the Urban Environmental Monitoring (UEM) STAR (Stefanov et al., 2001; Ramsey, 2003), as well as perhaps the most ambitious and complex, the global volcano STAR (Pieri and Abrams, 2004). The data used for this study were collected as part of the initial instrument calibration as well as the volcano STAR.

The instrument was designed and built in Japan, and therefore ASTER data are processed from level 0 (satellite) to level 1B (L1B, calibrated, geometrically corrected, radiance-at-sensor) in Japan and then delivered to the Land Processed Distributed Active Archive Center (LP-DAAC) in Sioux Falls, SD. This processing and shipping time can take up to 2 weeks and therefore is not ideal for immediate response to hazards such as volcanic eruptions. There exists, however, a mechanism whereby the United States science team can request emergency expedited data (up to five scenes per day) for natural disasters, hazards and/or important data collections. A minimum of 24 h are needed to create the new acquisition schedule and task of the instrument. However, once collected, these data are processed directly at the DAAC and available by way of file transfer protocol (ftp) in several hours (Ramsey and Dehn, 2002; Pieri and Abrams, 2004).

3. Volcanological background

3.1. Silicic dome surface morphology

The surface morphologies of silicic lava domes emplaced following a summit eruption are commonly short-lived with the dome either being destroyed by future eruptions or covered by continued effusion. Further, more subtle changes in the surface texture, composition and/or temperature can either signal new additions of lava, a change in the eruptive state, or the potential of further explosive activity (Anderson and Fink, 1990, 1992; Ramsey and Fink, 1999). Active monitoring of these domes becomes further complicated by heat and gas emissions as well as the threat of new eruptive events to researchers in the field. TIR remote sensing data such as those provided by ASTER are sensitive to textural, compositional, thermal, and atmospheric anomalies, and therefore provides a tool to observe and map these changes (Ramsey and Fink, 1999; Ramsey and Dehn, 2002; Byrnes et al., 2004).

Quantitative evaluation of thermal energy emitted from lava surfaces is complicated by the presence of the semi-amorphous glass that comprises the majority of most silicic domes and forms glassy rinds on flows of more mafic compositions (Crisp et al., 1990). The diagnostic spectral features characteristic of crystalline mineralogy are muted or commonly absent in glassy samples. Further, spectra from these samples are dramatically affected by the presence and abundance of surface roughness elements (i.e., vesicles) at the 10–100-μm scale (Ondrusek et al., 1993; Ramsey and Fink, 1999). These changes in spectral morphology can be used to decipher information about the composition and translate that into interpretations of volcanological processes occurring during lava emplacement. For example, previous studies have shown that vesicular textures are among the best indicators of the volatile distribution (and hence potential for explosive behavior) and the internal structure of silicic lava domes (Fink and Manley, 1987; Fink et al., 1992; Anderson et al., 1995; Ramsey and Fink, 1999). Whereas air photographs of the most silicic lavas allow qualitative assessment of these textures, such distinctions cannot be readily made for more mafic domes (dacite–andesite) and their collection at active volcanoes is commonly impossible. Furthermore, the VNIR–SWIR wavelength range is not sensitive to quantitative measures of vesicularity. Radar wavelengths provide the only other means to assess the distribution of roughness elements on lava flows and domes, but at the centimeter to meter (block-size) scale (Anderson et al., 1998). This change of four–six orders of magnitude in the roughness scale reveals information on volcanic processes that is very different than derived from the TIR region (Stofan et al., 2000).

The study of recently emplaced (<1 ka) silicic domes provides critical information on the dynamics and structure of their emplacement, serves as important test locales for remote sensing studies of their surface heterogeneities, and eliminates the complications of heat and gas discharge present on active domes. One technique to map the intimately mixed

textures and compositions on such lava surfaces is a linear spectral deconvolution approach (Ramsey and Christensen, 1998; Ramsey and Fink, 1999; Byrnes et al., 2004). Linear deconvolution of TIR spectra is based upon the well-tested assumption that energy emitted from a surface mixes linearly in direct proportion to the areal distribution of the end-members comprising that mixed spectrum. The choice of end-members can range from minerals to lithologic units to surface pumiceous textures depending on the objective of the study and the availability of data. Textural end-members used as inputs into such a model produce images that reveal subtle mixing patterns and allow for the areal distribution of those textures to be calculated (Ramsey and Fink, 1999). The work described here is the first application of ASTER data to the study of an active silicic dome (Bezymianny Volcano), which for most of 2000 was undergoing endogenic growth and subsequent collapse, forming small-scale pyroclastic flows and ash emissions (Ramsey and Dehn, 2002).

3.2. Volcanological activity at Bezymianny

Bezymianny is an andesitic to dacitic composite volcano, on the southern end of the Kliuchevskoi group of volcanoes (Fig. 2). It has been one of the most historically active volcanoes on the Kamchatkan Peninsula, producing dome-forming eruptions and less-common large ash plumes (Fedotov and Masurenkov, 1991). A catastrophic debris avalanche eruption in 1955–1956 ended a nearly 1000-year hiatus in activity (Gorshkov, 1959). This eruption alerted volcanologists to the dangers of debris avalanches and allowed identification of past debris avalanche deposits at other volcanoes (e.g. Sheveluch; Gorshkov and Dubik, 1970) well before the well-known debris avalanche at Mount St. Helens in 1980.

A large (>1 km in diameter) eastward facing amphitheater was created during the 1956 collapse at Bezymianny. Since this eruption, a series of lava domes have grown in the crater, with frequent directed blasts, collapses and ash plumes associated with cycles of dome destruction and growth (Fig. 3). Over the 10-year period from 1990 to 2000, the lava dome has been relatively stable with frequent low-level volcanic activity. On the average, Bezymianny has nearly two eruptive cycles per year typically in the

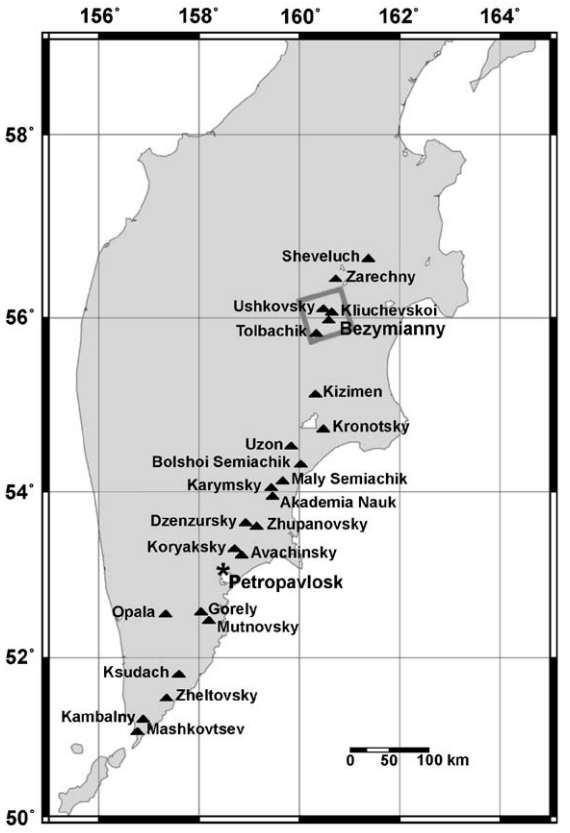

Fig. 2. Historically active volcanoes of the Kamchatkan Peninsula, Russia. The gray box is the approximate location and size of one ASTER scene (60 km × 60 km) located over the Kliuchevskoi Volcanic Group, which includes Bezymianny Volcano.

form of unrest at the lava dome. As new material is extruded, periods of fracture and collapse follow which can produce sub-Plinian eruption columns as well as block and ash flows into the valleys to the east and south of the volcano (Fig. 3).

During 2000, Bezymianny entered a period of enhanced activity punctuated by several larger eruption sequences. On 14 March 2000 the Kamchatka Volcanic Eruption Response Team (KVERT) raised the hazard level color code to red due to continuous volcanic tremor after a period of several days of increased seismicity (KVERT, 2000a). Moderate ash clouds (~ 7 km a.s.l.) were locally observed drifting to the NW. Several similar-sized eruptions occurred during the next week and were confirmed by local

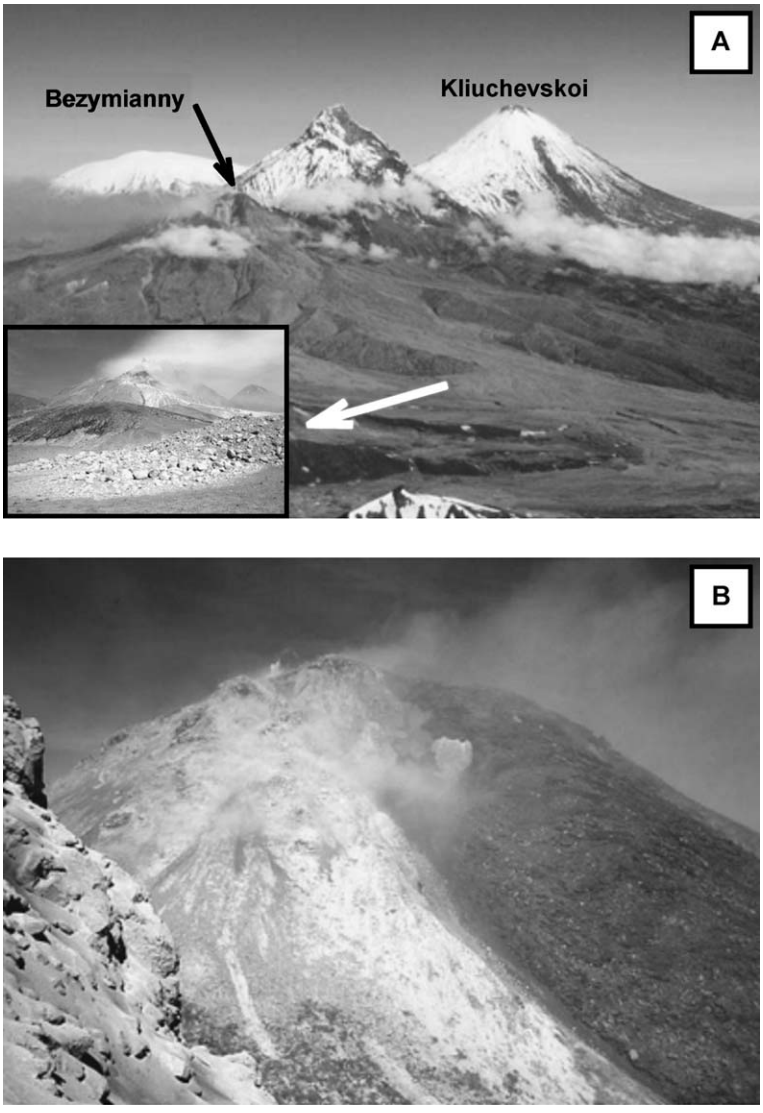

Fig. 3. Photographs of the Kliuchevskoi Volcanic Group, including Bezymianny Volcano (views looking north–northwest). (A) Older location photograph showing Bezymianny (indicated by the arrow) and its associated pyroclastic deposits in the foreground. Also visible to the north and right of Bezymianny are Kliuchevskoi and Ushkovsky Volcanoes, respectively. The inset photograph taken on 10 August 2001 from the general area indicated by the white arrow shows the typical block and ash flows that were deposited during the 2000–2001 eruptions. (B) Close-up photograph of the Bezymianny dome also taken on 10 August 2001, which shows a new lava flow erupted sometime in 2000 or 2001. Photographs courtesy of Michael Zelenski.

seismic monitoring. No significant activity was reported for the next 7 months and activity remained at normal background levels (GVN, 2000). However, local observations reported small fumarolic plumes that rose 50–300 m above the summit crater and drifted up to 10 km away. This style of activity is likely the normal background or restive state of Bezymianny, but is far below the detection limit of a system such as AVHRR.

By mid-October, fumarolic and seismic activity had increased once again. The hazard color code for the volcano was raised to yellow (GVN, 2000). By 25

October 2000 seismic data indicated that hot rock avalanches may have descended from the Bezymianny dome. B-type earthquakes increased 3 days later and by 31 October 2000 the most intense seismicity recorded that year took place. An ash plume extending ~ 80 km SE was observed indicating that a larger eruption had occurred. Intense seismicity was registered for the next several days and numerous small to moderate ash plumes were observed visually. Although volcanic ash advisory statements were issued to aviators during 2–3 November, the hazard status for Bezymianny decreased soon after and by 10 November 2000, the hazard color code was once again lowered to green (KVERT, 2000b).

4. Results

4.1. AVHRR

Since 1995, when the AVO satellite monitoring was initiated in this region, Bezymianny has not produced a large ash plume without first showing a thermal anomaly in AVHRR images (Dehn et al., 2000). However, it has produced thermal anomalies without subsequent plumes about 50% of the time as documented by Dehn et al. (2000). These have been interpreted as smaller extrusive dome growth episodes, which have not destabilized the dome. In 2000, Bezymianny had two eruptive cycles in March and September–November that produced observable thermal anomalies in the AVHRR images (Fig. 4). Activity in March increased and was monitored by both AVO and KVERT using the AVHRR thermal anomaly alert procedure. The first sequence produced thermal anomalies in AVHRR data a day before a dense dark plume rising to 5 km a.s.l. was reported by observers on 24 March 2000 (Fig. 5). No volcanic tremor was recorded during this ash event, and no ash signal was detected in GMS or AVHRR using the

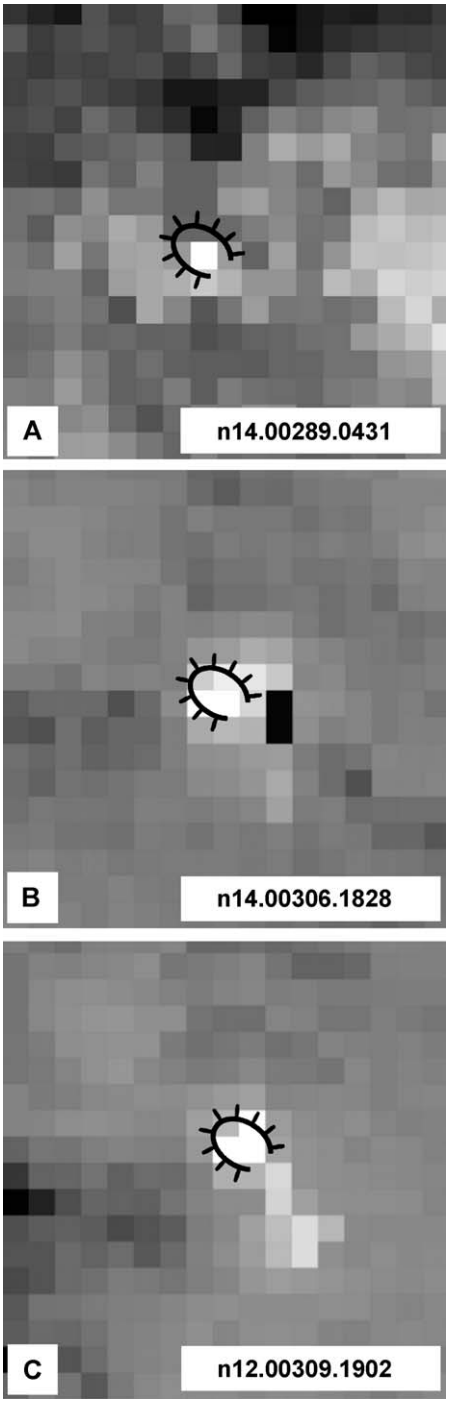

Fig. 4. Selected AVHRR data over Bezymianny Volcano in 2000. All images are north oriented to the top and are radiometrically and geospatially corrected, with a width of approximately 18 km (each pixel equal to 1.1 km). The bright shades of gray to white indicate higher pixel brightness temperatures. A graphical representation of the Bezymianny summit crater is overlain in each image. (A) 15 October 2000 image, a single pixel anomaly is seen. (B) 1 November 2000 image shows numerous saturated pixels centered on the dome (black pixel is a sensor recovery pixel that occurs after saturation). (C) 4 November 2000 shows a cooling of the dome with a spreading of the hot pixels indicating the flow deposit.

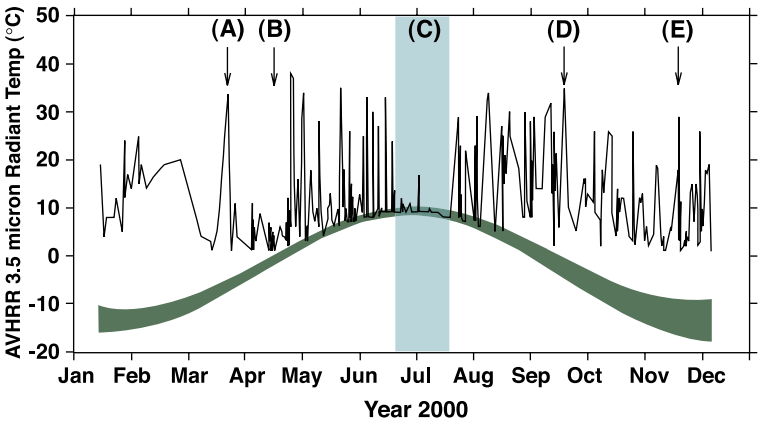

Fig. 5. Time versus radiant temperature plot for Bezymianny Volcano during 2000. The warmest pixel near or on the volcano in each nighttime cloud-free AVHRR pass is plotted. In general, the activity is heightened over the multiyear, non-volcanic background (plotted as the gray band). Although there is some structure to the plot, no definitive precursors are seen before the explosive bursts in March and October. Also shown are several significant events mentioned in the text including: (A) first AVHRR thermal anomalies detected by AVO (24 March); (B) first ASTER data collected (13 April); (C) summer quiescent period; (D) first AVHRR thermal anomalies for second eruptive cycle (21 September); (E) last AVHRR thermal anomaly for second eruptive cycle (12 November).

split-window technique (Prata, 1989; Schneider et al., 2000). This eruptive cycle was short lived, and ended days later.

The second eruptive cycle formally began after a thermal anomaly was noted in AVHRR data during the course of regular monitoring on 21 September 2000 (Fig. 5). Little or no seismic activity was detected during this period. The anomaly intensified over the following weeks and reached sensor saturation on 18 October 2000. At this time KVERT upgraded the level of concern color code from green to yellow. Seismicity remained low, though periodic low magnitude earthquakes suggest there were a few small hot rock avalanches from the lava dome during this time (KVERT, 2000b). A Landsat ETM+ image acquired on 15 October 2000 showed what appeared to be small ash or debris flows extending to the east and south of the lava dome. These flows were either cool at the time of emplacement or cooled extremely rapidly thereafter, because of the weak thermal anomalies present in the ASTER data from September to October (Fig. 6). These flows likely represent non-magmatic dome and/or talus collapse associated with the seismic activity. Seismicity increased during the last half of October, and on 30 October 2000, KVERT increased the level of concern to orange. AVHRR data still recorded persistent thermal anomalies at or near sensor saturation indicating that magmatic material was near the surface and an eruption was in progress. Later that day, a volcanic ash plume was detected drifting to southeast. Unfortunately, not all of the seismic stations were functioning at this time, underscoring the utility of remote sensing data to effectively monitor this volcano. After this, volcanic activity decreased, AVHRR monitoring recorded the last thermal anomaly on 12 November 2000, after which time the volcano once again entered a quiescent state as defined by the seismic and AVHRR satellite monitoring (GVN, 2000).

The size of AVHRR pixels, nominally 1.1 km on a side at nadir, precludes the detection of small-scale features and limits its reliability to evaluate in detail the volcanic processes. However, approximate temperatures for sub-pixel hot areas on the dome can be calculated using the dual-band approach (Dozier, 1981; Rothery et al., 1988; Harris et al., 1997). Simply stated, if the pixel-integrated thermal radiance is measured for two wavelengths, three unknowns are present: the temperatures of both the hot and cool surfaces as well as the fraction of the pixel radiating at the hot temperature (Dozier, 1981; Oppenheimer, 1991). The ratio of the hot to cool portions of the pixel is assumed to be proportional to the ratio of the hot and cold components of the total radiance (i.e., a linear relationship). However, these calculations require certain assumptions as to the geometry and

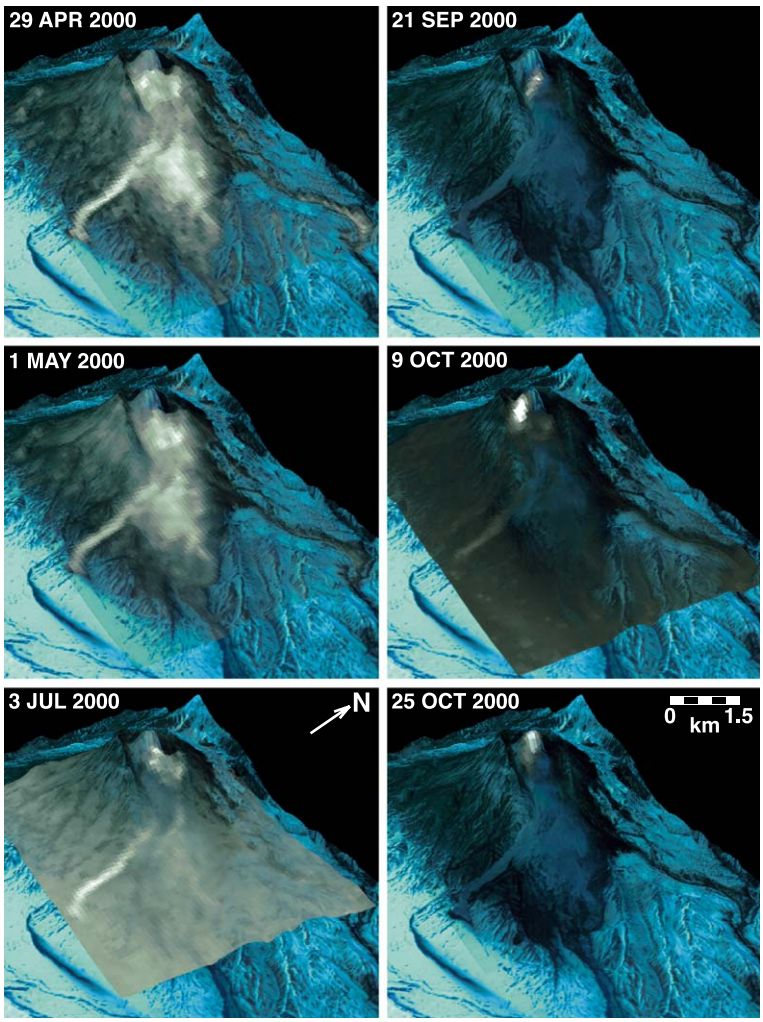

Fig. 6. Color composite three-dimensional drape of the ASTER 15 m/pixel VNIR image data over the ASTER-derived DEM (both from 1 May 2000). Over these are the TIR 90 m thermal anomaly data arranged in chronological order from April to October 2000. These images were chosen specifically to highlight both the non-eruptive (restive) behavior of the volcano during times where no AVHRR anomalies were seen (summer) as well as immediately following large eruptions (April and October). Significant changes in intensity and location of the anomalous pixels can be seen on the dome. Following the large eruption in March 2000 numerous hot debris flows were emplaced in the small valley southeast of the dome. This pattern occurred again following the October 2000 eruption (not shown here) and included two distinct flow emplacement/cooling events in 2 weeks at the end of December 2000/early January, 2001. This pattern likely represents endogenic lava dome growth and collapse following the larger eruptions.

thermal structure of the surface, which may or may not be accurate. For example, depending on the pixel size, which is variable across the AVHRR swath, the pixel's location with respect to the dome, and the accuracy of the temperature estimation of the background, errors as large as 200 °C are possible for the hot component. Further, because the AVHRR sensor saturates at 50 °C pixel-integrated temperature, this method breaks down completely for very hot and/or very large targets. These caveats necessitate that only a broad distinction in the type of activity can be made (i.e., is the activity phreatic or magmatic?) and the subsequent degree of monitoring response. For example, AVHRR data acquired on 4 November 2000 show

numerous pixels with elevated radiance (Fig. 4). Several of these pixels extend southeast from the dome complex, indicating the presence of flow deposition with elevated temperatures. Focusing on the pixels over the dome and using reasonable values for the dome area and background temperatures, the dual-band technique produces temperatures between 350 °C and 750 °C for the hot fraction. This wide range reflects the uncertainty of the technique as well as the possible variation in areal percentage of the hot regions in the pixel. Even where coupled with the possible 200 °C error mentioned above, these temperatures are still too high for phreatic activity, suggesting the exposure of fresh lava at the dome at this time.

In order to try to detect smaller changes in the thermal character of the volcano, time series data are provided by the *Okmok Algorithm* (Dean et al., 1998; Dehn et al., 2000). For Bezymianny volcano, a background curve of plausible temperatures during the year has been calculated. These data are filtered to accept cloud-free, nighttime passes only and are plotted against the actual temperatures recorded in thousands of successive AVHRR data sets in 2000 (Fig. 5). The activity at the volcano through 2000 is well above background, when compared to the usual annual temperature variation of previous years (Dehn et al., 2000). This high level of activity was not readily observed in the AVHRR data by analysts during 2000 and underscores the utility of this approach to detect states of unrest at volcanoes where voluminous background data sets exist. However, the high level of activity makes it difficult to interpret individual phases of the activity. A lull in activity seems to have started in mid-July (Julian Day 200) persisting through mid-August (Julian Day 226), then returning to the state of thermal unrest. It should be noted that no clear precursor or thermal change was seen preceding the explosive bursts of March or October (Fig. 5).

4.2. ASTER

During the eruption of Bezymianny in March–April 2000, the ASTER instrument was in orbit; however, it was still in an engineering validation period and therefore no data from this eruptive sequence were acquired. However, this activity did initiate the increased ASTER observations of the volcano beginning in mid-April and lasting for the next 9 months. ASTER was tasked to collect data over Bezymianny Volcano at every available opportunity focusing mainly on nighttime observations. This was a significant increase over the nominal STAR collection schedule of four scenes per year (Pieri and Abrams, 2004). Because ASTER continued in an instrument calibration/validation phase until October of that year, scientific data collection was a lower priority and off-nadir pointing was unavailable for most of that time. This did limit the total number of scenes collected, and for those that were successfully acquired, the pointing angle was minimal (Table 3). The resulting ASTER data collection interval over Bezymianny varied from 2 to 16 days. More than 20 ASTER scenes were collected, from which 14 were chosen for this analysis (Table 3). These data were mostly cloud free, centered on the volcano, contained minimal noise and showed obvious thermal anomalies. Initially, all scenes analyzed were calibrated (L1A or L1B) data; however, nearly all have been processed into various level 2 (L2) products such as surface radiance, emissivity and kinetic temperature (Abrams, 2000). All scenes were collected at night (SWIR and TIR sensors) with the exception of the 29 April and 1 May 2000 data sets. These were day acquisitions and as such had the full compliment of the sensors (VNIR–TIR), thereby allowing examination of the highest spatial resolution data and DEMs to be generated.

The night acquisitions took place near or around 11:00 UTC (23:00 local time) and displayed moderate to strong thermal anomalies centered on the summit dome complex. In some images the anomalies were also present down slope from the summit, indicating the presence of a cooling flow deposit (Fig. 6). In order to extract accurate kinetic temperatures from a multispectral TIR data set, the calibrated at-sensor radiance must first be corrected for atmospheric absorption, scattering, and emission. The resulting at-ground emitted radiance is described by the Planck equation, which is a function of the wavelength-dependant surface emissivity and the singular pixel-integrated brightness temperature (more detailed descriptions can be found in Realmuto, 1990 and Ramsey and Christensen, 1998). The unique separation of the emissivity values from temperature for any given pixel can only be performed if an under-deter-

Table 3
Subset of the processed ASTER scenes used in this analysis

ASTER Granule ID	Acquisition		Scene center	Pointing angle
	Date	Time (UTC)		
[a]SC:AST_L1B.003:2012482291	29-Apr-00	01:00:33	56.01°N, 160.25°E	8.56
[a,b]SC:AST_L1B.003:2012487838	1-May-00	00:48:16	55.90°N, 160.31°E	−5.71
SC:AST_L1B.003:2012638630	17-Jun-00	11:17:54	55.88°N, 160.73°E	−5.70
[a]SC:AST_L1B.003:2012770700	3-Jul-00	11:17:56	55.87°N, 160.68°E	−5.70
SC:AST_L1B.002:2006972460	4-Aug-00	11:16:56	55.89°N, 160.85°E	−5.70
SC:AST_L1B.002:2006972628	6-Aug-00	11:04:49	55.99°N, 160.86°E	5.70
SC:AST_L1B.002:2006972630	7-Sep-00	11:05:27	55.96°N, 160.64°E	8.55
[a]SC:AST_L1B.002:2006972631	21-Sep-00	11:17:19	55.86°N, 160.62°E	−5.70
[a]SC:AST_L1B.003:2003291467	9-Oct-00	11:04:24	55.98°N, 160.78°E	8.55
[a]SC:AST_L1B.003:2003402172	25-Oct-00	11:04:05	55.99°N, 160.81°E	8.55
SC:AST_L1A.003:2003588183	*3-Dec-00*	*11:09:10*	*56.18°N, 160.49°E*	*2.86*
SC:AST_L1B.003:2006972461	28-Dec-00	11:03:03	55.99°N, 160.82°E	8.55
SC:AST_L1A.003:2004074356	*4-Jan-01*	*11:09:02*	*56.16°N, 160.40°E*	*2.86*
SC:AST_L1BE.001:2002764666	11-Jan-01	11:14:47	55.81°N, 160.27°E	−2.86

[a] Scenes used for temperature and vesicularity images (Figs. 5 and 7).
[b] Day-time scene used for the background overlay and DEM shown in Figs. 5 and 7. All other scenes with the exception of 29 April 2000 were collected at night and show significant thermal anomalies.

mined system of equations is solved. For example, ASTER scans the surface over five wavelengths and therefore records five radiance values per pixel. Each radiance measurement is described by the Planck equation and contains two unknowns, the brightness temperature, which is invariant with wavelength, plus five wavelength-dependant emissivity measurements. The determination of these six unknowns must be done by making an assumption about either one of the emissivity values or the surface temperature, or by the introduction of ancillary data (Kahle, 1987; Realmuto, 1990; Gillespie et al., 1998). Numerous ASTER level 2 data products are now available including the surface emissivity and the kinetic temperature products (Gillespie et al., 1998; Abrams, 2000). The reader is referred to the aforementioned references or the ASTER home page (http://asterweb.jpl.nasa.gov/) for a complete description of the temperature–emissivity separation (TES) algorithm. A major component of the TES algorithm uses the normalized emittance technique similar to that described by Realmuto (1990). This technique attempts to solve the underdetermined system of radiance equations by assuming (for each pixel) a maximum emissivity for one of the instrument channels. That value can be allowed to vary up to the maximum physically possible value of 1.0. Realmuto (1990) found maximum emissivity values ranged from 0.95 to 0.99 for quartzite and basalt, respectively. A more detailed examination by Salisbury and D'Aria (1992) of over 60 samples spanning all compositions and rock types found an average of 0.983 ± 0.002. Ramsey and Fink (1994) described the error involved with such an assumption and how that error partitions into the results of a linear deconvolution of the emissivity data. They showed that a 5% error in the assumption of the maximum emissivity resulted in approximately 1% error in the retrieved temperature and a $<0.5\%$ error in the final deconvolution end-member results.

The L2 kinetic temperature and emissivity data products were examined for the ASTER TIR scenes of Bezymianny Volcano and the surrounding area (Table 3). Six of these images spanning the first six months of ASTER observations are shown in Fig. 6. Each image is a composite of the 90-m TIR nighttime data with brighter pixels indicating stronger thermal anomalies (hotter pixels) overlain onto the 1 May 2000 VNIR data and derived DEM (both at 15 m spatial resolution). The summit crater and dome complex are in the upper part of each image and the primary depositional channel extends approximately 5 km to the south, southeast of the dome (see Fig. 3). Throughout the summer observation period between the larger eruptions of March and October, every ASTER TIR image showed some level of increased thermal anomalies on the dome complex, none of

which was detected by AVHRR. In some cases, these thermal anomalies were only one ASTER pixel (90 × 90 m) and therefore assumed to be caused by a sub-pixel heat source, such as an active fumarole. In other scenes, a large portion of the dome surface is slightly elevated in temperature, indicating an overall heating of the dome (i.e., 3 July 2000).

The high radiometric accuracy of the ASTER TIR subsystem coupled with 90-m pixels allows for 1–2 °C detection threshold, much smaller than the more than 5 °C needed for AVHRR (Dean et al., 2002b). For all the anomalies during the summer period, the temperature range was 2–15 °C above the average background, which cooled from 15 to 5 °C from early June to late September. These warmer pixels moved dramatically over the entire 9 months of ASTER data collection, perhaps indicating the cooling of existing fumaroles and the onset of new ones, or the warming of the dome carapace in response to endogenic dome growth. With the exception of the 9 October 2000 scene, the relatively low temperatures and the confinement of the anomalies to several pixels, it is doubtful that this behavior indicated the emplacement of new lava on the surface (Harris et al., 2001). The activity observed with ASTER during this time could represent either normal activity at Bezymianny, or the final stages of the March eruptive cycle. These changes are too small to be detected by routine AVHRR monitoring, but could provide valuable information on the state of unrest at a volcano prior to a large eruption. Also detectable with ASTER were thermal anomalies extending south into the primary drainage valleys. These elevated temperature regions likely indicate the presence of cooling debris flows and are particularly evident in images acquired in April–July (Fig. 6) and again in late 2000 following the larger eruptions in October of that year.

Beginning in late September, the volcano entered a period of increased activity and thermal anomalies were again detected by AVHRR as well as ASTER (Figs. 5, 6). For the stronger anomalies on the dome, the ASTER pixel-integrated temperatures on 9 October 2000 were slightly below the TIR saturation threshold of 100 °C. The anomalies also showed a concentration and localization in the south-central portion of the dome, possibly indicating a fracturing of the dome carapace and/or the emplacement of new lava on the surface (Fig. 6). As mentioned, AVHRR saturates above pixel-integrated temperature of 50 °C (SWIR) and ASTER above 100 °C (TIR). These saturated pixels in AVHRR likely reflect the presence of magmatic temperatures and are generally assumed to indicate an eruption in progress. The strongest recorded thermal anomaly detected by ASTER was 92.5 °C on 9 October 2000 (~ 109 °C above the background temperature on the summit). These dome temperatures steadily decreased with time to ~ 50 °C and ~ 13 °C on 25 October 2000 and 11 January 2001, respectively, as the volcano once again entered another restive state.

Following the onset of larger eruptions in late September 2000 and continuing through to January 2001, Bezymianny entered a period of dome collapse and subsequent pyroclastic flow emplacement. The thermal anomalies present on the dome surface also resumed the pattern of seemingly random movement. The flow deposits were confined to the valley south of the summit dome complex and their warmer temperatures were easily detected with ASTER TIR (Fig. 6). The kinetic temperature of the deposits varied from 1.5 °C to 2.5 °C above background in October when the primary activity was concentrated on the dome. Following emplacement of a large flow deposit in December, detected temperatures were 6 °C to 10 °C above background. Fig. 6 shows an example of this behavior from the earlier eruptions of 2000, with the presence of a warm flow seen in the April–July 2000 images and little to no thermal anomaly present later in the summer and fall. This cyclic nature of dome warming, collapse, and subsequent hot flow emplacement/cooling was monitored by ASTER in late 2000/early 2001 long after AVHRR detected thermal anomalies and the volcano color code returned to green (KVERT, 2000a).

As mentioned, calibrated thermal infrared radiance is a function of both the temperature and surface emissivity. ASTER has five TIR bands making it the first civilian sensor with multispectral TIR capabilities. This design provides the means to model and map not only the temperature of the surface, but also the chemical composition (petrology) and the surface roughness (vesicularity). Ramsey and Fink (1999) have shown that multispectral TIR emissivity can be used to estimate the percentage of vesicles (or the micron-scale roughness) on the surface of Holocene silicic domes using a relatively straightforward linear

deconvolution approach. By modeling the emissivity spectrum derived from each pixel on the dome surface as a combination of glass and featureless blackbody emission (a proxy for vesicles and roughness elements) they showed that vesicularity could be estimated to within 5% under ideal situations. Even more importantly, it was speculated that changes in the vesicle amount and location on the dome could indicate the emplacement of new lava and the potential for further dome collapse. The ASTER L2 emis-

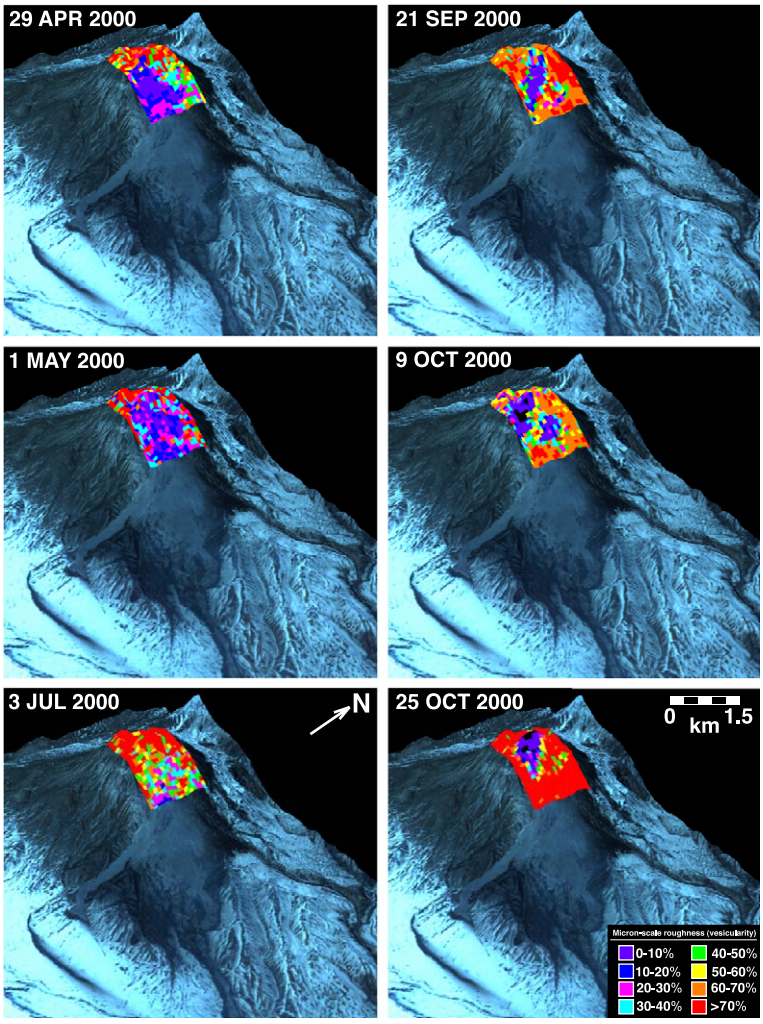

Fig. 7. Same color composite/DEM drape and time period as shown in Fig. 6. However, here a small image subset of the micron-scale roughness (vesicularity) modeled from the ASTER TIR data is overlain on the Bezymianny dome. See text and Ramsey and Fink (1999) for a detailed explanation of the deconvolution modeling technique. Although the model results are highly variable, certain spatial and temporal patterns can be seen. Large, low micron-scale roughness (<20%) regions are present on the dome and correspond to the regions of highest thermal output. These regions likely contain very strong sub-pixel temperature mixing during or immediately following the larger eruptions. This mixing causes an inaccurate emissivity retrieval and therefore low modeled values that become negative (black pixels) in extreme circumstances. With time following the eruption in March 2000, the roughness of the dome trends higher as sub-pixel temperature is no longer present and potentially new surface flows become less rough at the micrometer scale through surface weathering and vesicle infilling by airborne ash and/or particulates. This progression is reset in September and October when the dome is subject to a new cycle of heating, eruption and potentially new surface flows.

sivity product for the same dates displayed in Fig. 6 was subjected to the deconvolution model using a laboratory-derived silica-rich obsidian glass spectrum and the spectrum of a blackbody as end-members. This represents the first time this approach has been applied to an actively erupting silicic dome. The results for the model are color coded and shown in Fig. 7. For each image, the micron-scale roughness of the dome varied from 2% to 74%, with an average value of approximately 40%. Statistically significant low (<20%) and high (>60%) values were present on the dome and surrounding talus slopes. Much of the area corresponding to the highest values corresponds to the talus and may represent fine-grained mantling material (ash) and/or surface weathering over time. In addition, the high values on the 25 October 2000 image correspond to low-level cirrus clouds present at an elevation slightly below the dome. Concentrated in the region of strongest thermal anomalies, the model is returning low values of micron-scale roughness. This could be due to either of two effects or the combination of both. These regions may correspond to newly emplaced, highly degassed lava, which is being extruded onto the surface of the dome. Similar densely microcrystalline lavas are present as late-stage extrusions on many of the silicic domes in the southern Cascades in the western United States (Sampson, 1987; Fink and Manley, 1987). Alternatively, the low values could be caused by recovered emissivity spectra that are distorted due to sub-pixel temperature mixing. The mixing of a small fraction of very hot surface with a large fraction of cool surface in a pixel results in an overall radiant energy flux that can no longer be solved with a simple inversion of the Plank equation and separation of emissivity from temperature. Commonly, this is manifest as a negative slope toward longer wavelengths in the recovered emissivity spectra, which results in impossibly low values (0.2–0.5). If this effect is large enough, the entire spectrum for a given pixel can be depressed below the glass end-member spectrum and the resulting deconvolution model fit would be a negative roughness or vesicularity value. This occurs in the 9 October and 25 October images and shown as black pixels in Fig. 7. Recall, that this is also the time frame of renewed eruptive activity at Bezymianny and the detection of numerous thermal anomalies by AVHRR. It is entirely plausible that these pixels have small fractions of very hot material being exposed during a phase of exogenic dome growth. In theory, the magnitude of this temperature mixing can be estimated from the data and a near-accurate reconstruction of emissivity spectrum is possible. This has not been attempted here because it is beyond the scope of the initial research. However, it is being explored by the authors and a model to extract sub-pixel temperatures as well as micron-scale roughness is being developed.

5. Discussion

Clearly, satellite data with the resolution of AVHRR are sufficient to detect renewed activity at a volcano and can be used to place constraints on the magnitude of that activity. Where combined with local seismic and human observations, low spatial resolution satellite data can also be correlated to some of the actual eruptive processes ongoing at a particular volcano. However, these ancillary data sets are not always available at every volcano, thereby limiting the usefulness of sensors like AVHRR and GOES to monitoring tools for the most part. Having the ability to combine an operational monitoring effort with high-resolution satellite data provides nearly complete coverage of the volcanic processes ongoing during both the eruptive and (perhaps even more importantly) the non-eruptive periods. Such observations over the week to month time scale can provide an excellent baseline on these processes, which could include dome cooling or warming (caused by a decrease or increase in magma flux, respectively); contraction, expansion and/or fracturing; fumarolic variability; as well changes in the surface roughness. Further, where monitored anomalies strongly deviate from this baseline, new summit activity can be assumed to have occurred.

This style of activity and surface change is seen at Bezymianny Volcano throughout the summer quiescent period (so called by the lack of AVHRR anomalies) where numerous low-grade thermal and vesicularity changes were noted by ASTER. In addition, at least one nighttime ASTER image shows a very small ash plume extending approximately 30 km from the summit, indicating that even during these non-eruptive phases, volcanoes such as Bezymianny continue to evolve and remain in a state of activity

despite a color green color code. The movement of these low-grade thermal anomalies is most likely controlled by the availability of surface water and the creation of new fractures due to endogenous dome growth. However, such anomalies could never before be measured with such precision from space. The 90-m spatial resolution of the ASTER TIR sensor combined with its low noise equivalent delta temperature (NEΔT) allows pixel-integrated thermal anomalies to be resolved that are only a few degrees Celsius above the background. Such small anomalies could represent a significant fumarolic zone on a dome. For example, if a small region on the dome of Bezymianny covering only 0.10% of an ASTER TIR pixel ($\sim 8m^2$) is elevated to 500 °C above an average background temperature of 5 °C, the resulting pixel-integrated kinetic temperature would be ~8.5 °C. This relatively large, hot region could be important in understanding the dome's hazard state and volatile evolution, but would never be detected by routine AVHRR monitoring.

As Bezymianny transitioned back into an actively erupting state, AVHRR again detected thermal anomalies starting 21 September 2000 and lasted until 12 November 2000. This was the period of increased eruptive activity, small to moderate steam and ash plumes, as well as moderate seismicity. The saturation of AVHRR pixels on 9 October and 18 October 2000 indicated the probability that magmatic activity was occurring at the surface, and where coupled with low magnitude earthquakes suggested that small rock avalanches were occurring, which prompted an eruption alert by KVERT on 30 October 2000 (KVERT, 2000b). The higher resolution ASTER data acquired on 9 October 2000 contained one pixel with a maximum kinetic temperature of 92.5 °C. This was more than 90 °C above the temperature of the surrounding region and a significant change from the thermal state of the dome observed by ASTER 2 weeks prior. Upon degradation of the 90-m ASTER TIR spatial resolution to the 1.1 km of AVHRR, the maximum kinetic temperature decreased from 92.5 °C to 63 °C, thereby validating the saturation of AVHRR (Ramsey and Dehn, 2002).

The weaker anomalies observed throughout the summer disappeared almost entirely prior to the larger eruptions in late October (Fig. 6). The increased thermal output and pressurization of the dome during the eruption could have shut down the fumarolic system. This thermal output was confined to a linear fracture zone in the central southern flank of the dome, which represents the exposure of near magmatic temperatures at the surface. It was present throughout October to mid-November, although it diminished in intensity. The region of the dome surrounding the large anomaly was also elevated in temperature and could represent endogenous growth, with subsequent carapace fracturing and instability of the dome. It was an area of anomalously low vesicularity model results and appears to be the source region for pyroclastic flow material. These flows were deposited in the small southeastern-trending valley demarcated by elevated temperatures from November 2000 to January 2001. The magnitude and shape of those thermal anomalies were similar to the ones from May to July 2000 (Fig. 6). However, unlike temperature data from that period, the data from late 2000 showed no larger deposits on the eastern flank. This indicates that the October 2000 eruptions were smaller than those that occurred in March and the subsequent pyroclastic flows likely occurred from localized dome collapse and rock fall.

It is clear in the ASTER data that weak, quickly cooling thermal anomalies are present in the valleys below the dome of Bezymianny. These flow deposits were routinely detected by ASTER and only on rare occasions by AVHRR. The question arises as to the nature of these deposits and what they reveal about the ongoing eruptive processes at Bezymianny. In order to better answer these questions, the recent history of the volcano can be examined. Beginning in 1960, several years after the large edifice collapse eruption, block and ash pyroclastic flows started accompanied by the growth of the lava dome (Girina et al., 2002). The first viscous lava flow was observed on the dome in February 1977, and a new phase of activity began that year, which consisted of dome growth, ash explosions, small lateral directed blasts and pyroclastic flows, followed by the extrusion of viscous lava flows.

The past activity at Bezymianny indicates that pyroclastic flows are favored over lahars because a large source of water is lacking. For a large portion of the year snow is present; however, the volcano is not capped by summit glaciers. This can be further constrained by examination of the ASTER TIR data. The deposits have a relatively large (~ 10 °C above background) initial thermal anomaly, indicating the

presence of quite hot material over large portions of the surface. However, these deposits also have a subsequent high cooling rate, which indicates a low density, low thermal inertia material such as ash and/or highly pulverized material rather than rock or indurated mud. The lower thermal inertia of a block and ash deposit would allow it to cool quickly despite having a high initial temperature. A higher density lahar deposit on the other hand should retain the residual heat longer than 1 week. ASTER also has the ability to determine composition as well as the temperature of volcanic surfaces. Examination of the ASTER-derived vesicularity and spectral morphology (composition) of the flow deposits in the valley showed they were very similar to the dome surface, indicating that the material was likely derived from collapse of the dome itself. Finally, the associated small ash plumes observed during this period are commonly associated with pyroclastic flow emplacement rather than lahars.

Whereas the temperature data are critically important in understanding the ongoing processes at active lava domes, the ability of ASTER to map and monitor the chemical changes of the gas, sublimates and lava is even more significant. This combination gives volcanologists a much more powerful tool than any previous satellite instrument. For example, this study represents the first application of micron-scale textural mapping using TIR remote sensing on an active dome (Fig. 7). Highly variable surface roughness is strongly correlated with the regions of increased thermal radiance during the large eruptions. These regions may represent the emplacement of vesiculated or scoriaceous lava similar to lobes seen at the Mt. St. Helens dome following the 1980 eruption (Anderson and Fink, 1990) or highly degassed, dense lava similar to those seen on domes in the Cascades and at Mt. Unzen, Japan (Sampson, 1987; Nakada et al., 1995). Because the deconvolution technique is sensitive to changes in the depth and morphology of the glass absorption feature in the emissivity spectrum, other processes that result in an artificial increase (i.e., sub-pixel temperature mixing) or decrease (i.e., thin clouds or fine-grained particles) in the spectral contrast will impact the model results. For example, the 25 October 2000 image shows an apparent increase in the derived vesicularity values surrounding the dome, but this is due to the presence of thin cirrus clouds (Fig. 7). These complicating effects necessitate caution in interpretation of the model results. However, examination of other data sets such as the root-mean-squared (RMS) error image produced by the deconvolution model, the associated kinetic temperature, as well as the VNIR images (if present), commonly allows for separation of these complicating effects. In other cases, an understanding of volcanic processes can assist in resolving ambiguities. If a localized region of apparent high vesicularity is resolved, it may be caused by processes other than actual emplacement of vesiculated lava, such as the presence of ash fall or deposition of minerals associated with fumarolic activity. However, ash fall generally does not occur in areally distinct patterns. And whereas the deposition of fine-grained minerals surrounding fumaroles is also common, their formation should also be areally associated with higher thermal anomalies and have distinguishing spectral features than the dome surface. Further, the rapid change of surface spectra observed on Bezymianny's dome would require the deposition and removal of these minerals to be extremely quick, on the order of days to weeks. Regardless of the root-cause, the deconvolution approach is clearly delineating the presence of surface changes on the dome that correlate to changes in thermal activity and the onset of new eruptive activity.

6. Conclusions

Magmatic activity increased significantly at Bezymianny Volcano in the last half of 2000. Thermal anomalies detected in AVHRR images in mid-March of that year provided the first satellite observations of renewed activity. Both plumes and new dome formation were detected and KVERT issued its highest alert warning (GVN, 2000). Numerous AVHRR thermal anomalies, pyroclastic flows, and plumes extending 10–20 km from the summit were observed. At this time, a request was made to increase the observational frequency of the recently launched ASTER instrument for Bezymianny Volcano. For the next 9 months, ASTER collected over 20 scenes, which have been used to further monitor the eruption, make comparisons to the AVHRR data, and produce vesicularity and temperature maps of the dome.

This study provided the first high-spatial/multispectral resolution TIR observations of an actively erupting dome over several months during both the day and night, and in some cases with repeat times of only 2 days. It deviates significantly from other studies using space-borne TIR data of silicic domes. For example, in a detailed study Harris et al. (2002) use the TIR band of the ETM+ instrument to examine the thermal properties of the Santiaguito lava dome in Guatemala. That study examined only three TIR scenes collected over 3 years and cannot extract emissivity information, because of the singular TIR band. In comparison, this work using ASTER has a much higher temporal and spectral resolution, and captures two larger eruptive periods at Bezymianny as well as the restive state following each. The results have important bearing on the cyclic nature of the dome heating, eruption and subsequent collapse.

The high radiometric accuracy of the ASTER data allowed anomalies of less than 2 °C above background to be detected and monitored. This significantly decreases the detection threshold and effectively allows ASTER to be used as a monitoring tool for the low-grade background behavior, which is common for many volcanoes in the northern Pacific region. The ASTER data detected thermal anomalies covering tens to hundreds of pixels from April 2000 to January 2001 (much longer than either AVHRR or Landsat ETM+ data have shown). These data are clearly highlighting the eruptive activity by showing the movement of anomalies with a concentration along a fissure prior to larger eruptions of October–November. That eruption was also detected by AVHRR and resulted in the formation of a hot flow deposit seen in the subsequent months by ASTER. This represents the first time such an instrument was used for a dedicated long-term observation of active lava dome processes. The combined use of the new EOS technology with a proven monitoring system for volcanic eruptions appears to be very successful, allowing both the initial eruption alerts and detailed follow-up measurements to be made from space.

High-resolution data such as those from ASTER are critical for volcanic studies in that they allow for the discrimination of smaller thermal, textural, and compositional anomalies on the surfaces of lava flows and domes. However, even during eruptions where ASTER is in an increased acquisition mode, the repeat time is not sufficient for its use strictly as a monitoring tool. For that objective, a higher temporal resolution instrument such as AVHRR must be utilized at the expense of capturing any of the small-scale activity of the volcano. Clearly, having an instrument like ASTER with the temporal resolution of AVHRR would be ideal, but such a system is not likely in the near future. In fact, there are no plans for a follow-on sensor like ASTER on future NASA satellites or to extend the technology of high spatial resolution multispectral TIR for other spaceborne observations. Sadly, the opposite trend is true with even the single TIR band being eliminated on the future Landsat follow-on mission. Therefore, even though ASTER is the first instrument to have such capabilities and is proving to be an extremely valuable tool for numerous scientific studies including volcanic processes, it may be the last of its kind for many years.

In order to take advantage of the ASTER data while they exist, plans are now underway to utilize the existing AVHRR monitoring as a trigger for ASTER emergency data requests (Ramsey and Dehn, 2002). This would lead to a cooperative infrastructure between the ASTER science team and the AVO research scientists, providing ASTER data to the AVO analyst within hours after collection with little to no human intervention. And because AVO has a monitoring program in place with AVHRR, the combination of that instrument's high temporal resolution with the high spatial/spectral resolution of ASTER provides the best case scenario using available instruments. If successfully linked into an automated eruption monitoring program, the synergy would be ideal for studying nearly all facets of explosive volcanic eruptions, and mitigating the associated hazards.

Acknowledgements

The authors would like to thank Rick Wessels and Matt Patrick for assistance with initial data collection, calibration and analyses of ASTER and AVHRR, respectively. Olga Girina and Michael Zelenski provided the photographs of Bezymianny Volcano taken during a field trip in August 2001. In addition, Olga Girina provided helpful comments on the general nature of the recent activity at Bezymianny. Finally, very helpful and detailed reviews were

provided by Luke Flynn and Peter Mouginis-Mark, which resulted in substantial revisions to the manuscript and a much improved work. This research is supported under the NASA Solid Earth and Natural Hazards Program (NAG5-9439) as well as the ASTER Science Project.

References

Abrams, M., 2000. The Advanced Spaceborne Thermal Emission and Reflectance Radiometer (ASTER): data products for the high spatial resolution imager on NASA's Terra platform. Int. J. Remote Sens. 21, 847–859.

Anderson, S.W., Fink, J.H., 1990. The development and distribution of lava textures at the Mount St. Helens dome. In: Fink, J.H. (Ed.), Lava Flows and Domes: Emplacement Mechanisms and Hazard Implications. IAVCEI Proc. Volc., vol. 2, pp. 25–46.

Anderson, S.W., Fink, J.H., 1992. Crease structures: indicators of emplacement rates and surface stress regimes of lava flows. Geol. Soc. Am. Bull. 104, 615–625.

Anderson, S.W., Fink, J.H., Rose, W.I., 1995. Mount St. Helens and Santiaguito lava domes: the effect of short-term eruption rate on surface texture and degassing processes. J. Volcanol. Geotherm. Res. 69, 105–116.

Anderson, S.W., Stofan, E.R., Plaut, J.J., Crown, D.A., 1998. Block size distributions on silicic lava flow surfaces: implications for emplacement conditions. Geol. Soc. Am. Bull. 110, 1258–1267.

Bishop, M.P., Kargel, J.S., Kieffer, H.H., MacKinnon, D.J., Raup, B.H., Shroder, J.F., 2000. Remote sensing science and technology for studying glacier processes in high Asia. Ann. Glaciol. 31, 164–170.

Byrnes, J.M., Ramsey, M.S., Crown, D.A., 2004. Surface unit characterization of the Mauna Ulu flow field, Kilauea Volcano, Hawai'i, using integrated field and remote sensing analyses. J. Volcanol. Geotherm. Res. 135, 169–193 (this issue).

Crisp, J., Kahle, A.B., Abbott, E.A., 1990. Thermal infrared spectral character of Hawaiian basaltic glasses. J. Geophys. Res. 95, 21657–21669.

Dean, K.G., Servilla, M., Roach, A., Foster, B., Engle, K., 1998. Satellite monitoring of remote volcanoes improves study efforts in Alaska. EOS Trans. Am. Geophys. Union 79 (413), 422–423.

Dean, K.G., Dehn, J., McNutt, S., Neal, C., Moore, R., Schneider, D., 2002a. Satellite imagery proves essential for monitoring erupting Aleutian volcano. EOS Trans. Am. Geophys. Union 83 (243), 246–247.

Dean, K.G., Dehn, J., Engle, K., Izbekov, P., Papp, K., Patrick, M., 2002b. Operational satellite monitoring of volcanoes at the Alaska Volcano Observatory. Adv. Environ. Mon. Mod. 1 (3), 70–97.

Dehn, J., Dean, K.G., Engle, K., 2000. Thermal monitoring of North Pacific volcanoes from Space. Geology 28, 755–758.

Dozier, J., 1981. A method for satellite identification of surface temperature fields of subpixel resolution. Remote Sens. Environ. 11, 221–229.

Fedotov, S.A., Masurenkov, Y.P., 1991. Active Volcanoes of Kamchatka, vol. 1. Nauka, Moscow.

Fink, J.H., Manley, C.R., 1987. Origin of pumiceous and glassy textures in rhyolite flows and domes. In: Fink, J.H. (Ed.), The Emplacement of Silicic Domes and Lava Flows. Spec. Pap. Geol. Soc. Am. 212, 77–88.

Fink, J.H., Anderson, S.W., Manley, C.R., 1992. Textural constraints on effusive silicic volcanism: beyond the permeable foam model. J. Geophys. Res. 97, 9073–9084.

Flynn, L.P., Wright, R., Garbeil, H., Harris, A.J., Pilger, E., 2002. A global thermal alert system using MODIS: initial results from 2000–2001. Adv. Environ. Mon. Mod. 1 (3), 37–69.

Gillespie, A.R., Matsunaga, T., Rokugawa, S., Hook, S.J., 1998. Temperature and emissivity separation from Advanced Spaceborne Thermal Emission and Reflection Radiometer (ASTER) images. IEEE Trans. Geosci. Remote Sens. 36, 1113–1126.

Girina, O., Ozerov, A., Nuzhdina, I., Zelenski, M., 2002. The eruption of Bezymianny volcano on August 7, 2001. In: Dehn, J.D. (Ed.), Proc. 3rd Ann. Subduction Proc. Kurile–Kamchatka–Aleutian Arcs. Univ. Alaska, Fairbanks, AK, pp. 104–105.

Glaze, L.S., Francis, P.W., Rothery, D.A., 1989. Measuring thermal budgets of active volcanoes by satellite remote sensing. Nature 338, 144–146.

Global Volcanism Network (GVN), D.A., 2000. Bezymianny Volcano. Smithson. Inst. Bull. Global Volcanol. Netw. 25 (4), 8–9.

Gorshkov, G.S., 1959. Gigantic eruption of Bezymianny Volcano. Bull. Volcanol. 20, 77–109.

Gorshkov, G.S., Dubik, Y.M., 1970. Gigantic directed blast at Shiveluch Volcano, Kamchatka. Bull. Volcanol. 34, 261–288.

Harris, A.J.L., Butterworth, A.L., Carlton, R.W., Downey, I., Miller, P., Navaro, P., Rothery, D.A., 1997. Low-cost volcano surveillance from space: case studies from Etna, Krafla, Cerro Negro, Fogo, Lascaar and Erebus. Bull. Volcanol. 59, 49–64.

Harris, A.J.L., Flynn, L.P., Keszthelyi, L., Mouginis-Mark, P., Rowland, S.K., Resing, J.A., 1998. Calculation of lava effusion rates from Landsat TM data. Bull. Volcanol. 60, 52–71.

Harris, A.J.L., Wright, R., Flynn, L.P., 1999. Remote monitoring of Mount Erebus Volcano, Antarctica, using polar orbiters: progress and prospects. Int. J. Remote Sens. 20, 3051–3071.

Harris, A.J.L., Pilger, E., Flynn, L.P., Garbeil, H., Mouginis-Mark, P., Kauahikaua, J., Thornber, C., 2001. Automated, high temporal resolution, thermal analysis of Kilauea volcano, Hawai'i, using GOES satellite data. Int. J. Remote Sens. 22, 945–967.

Harris, A.J.L., Flynn, L.P., Matias, O., Rose, W.I., 2002. The thermal stealth flows of Santiaguito Dome, Guatemala: implications for the cooling and emplacement of dacitic block-lava flows. Geol. Soc. Am. Bull. 114, 533–546.

Kahle, A.B., 1987. Surface emittance, temperature, and thermal inertia derived from thermal infrared multispectral scanner (TIMS) data for Death Valley, California. Geophysics 52, 858–874.

Kahle, A.B., Palluconi, F.D., Hook, S.J., Realmuto, V.J., Bothwell, G., 1991. The Advanced Spaceborne Thermal Emission and Reflectance Radiometer (ASTER). Int. J. Imaging Syst. Technol. 3, 144–156.

Kamchatka Volcanic Eruption Response Team (KVERT) Report, 2000a. Bezymianny Volcano, March–April (http://www.avo.alaska.edu/avo4/updates/kvrtma00.html).

Kamchatka Volcanic Eruption Response Team (KVERT) Report, 2000b. Bezymianny Volcano, September–October (http://www.avo.alaska.edu/avo4/updates/kvert_000910.html).

Kaufman, Y.J., Herring, D.D., Ranson, K.J., Collatz, G.J., 1999. Earth Observing System AM1 mission to earth. IEEE Trans. Geosci. Remote Sens. 36, 1045–1055.

Kieffer, H.H., Frank, D., Friedman, J.D., 1981. Thermal infrared surveys at Mount St. Helens—Observations prior to the eruption of May 18. In: Lipman, P.W., Mullineaux, D.R. (Eds.), The 1980 Eruptions of Mount St. Helens, Washington. USGS Professional Paper 1250. U.S. Government Printing Office, Washington, DC, pp. 257–277.

Miller, T.P., Casadevall, T.J., 2000. Volcanic ash hazards to aviation. In: Sigurdsson, H., Houghton, B., McNutt, S.R., Rymer, H., Stix, J. (Eds.), Encyclopedia of Volcanoes. Academic Press, San Diego, CA, pp. 915–930.

Nakada, S., Miyake, Y., Sato, H., Oshima, O., Fujinawa, A., 1995. Endogenous growth of dacite dome at Unzen volcano (Japan), 1993–1995. Geology 13, 157–160.

Ondrusek, J., Christensen, P.R., Fink, J.H., 1993. Mapping the distribution of vesicular textures on silicic lavas using the Thermal Infrared Multispectral Scanner. J. Geophys. Res. 98, 15903–15908.

Oppenheimer, C., 1991. Lava flow cooling estimated from Landsat Thematic Mapper Infrared data: the Lonquimay eruption (Chile, 1989). J. Geophys. Res. 96, 21865–21878.

Oppenheimer, C., 1993. Infrared surveillance of crater lakes using satellite data. J. Volcanol. Geotherm. Res. 55, 117–128.

Pieri, D.C., Abrams, M.J., 2004. ASTER watches the world's volcanoes: a new paradigm for volcanological observations from orbit. J. Volcanol. Geotherm. Res. 135, 13–18 (this issue).

Prata, A.J., 1989. Observations of volcanic ash clouds in the 10–12 micron window using AVHRR 2 data. Int. J. Remote Sens. 10, 751–761.

Ramsey, M.S., 2003. Mapping the City Landscape From Space: The Advanced Spaceborne Thermal Emission and Reflectance Radiometer (ASTER) Urban Environmental Monitoring Program. In: Heiken, G., Fakundiny, R., Sutter, J. (Eds.), Earth Science in the Cities. Am. Geophys. Union, Washington, DC, pp. 337–361.

Ramsey, M.S., Christensen, P.R., 1998. Mineral abundance determination: quantitative deconvolution of thermal emission spectra. J. Geophys. Res. 103, 577–596.

Ramsey, M.S., Dehn, J., 2002. The 2000 eruption of Bezymianny Volcano captured with ASTER: a proposal to integrate high-resolution remote sensing data into real-time eruption monitoring at AVO. In: Dehn, J.D. (Ed.), Proc. 3rd Ann. Subduction Proc. Kurile–Kamchatka–Aleutian Arcs. Univ. Alaska, Fairbanks, AK, pp. 106–107.

Ramsey, M.S., Fink, J.H., 1994. Remote monitoring of volcanic domes: detection of chemical, textural and thermal heterogeneities (abstract). Trans. Am. Geophys. Union 75, 716.

Ramsey, M.S., Fink, J.H., 1999. Estimating silicic lava vesicularity with thermal remote sensing: a new technique for volcanic mapping and monitoring. Bull. Volcanol. 61, 32–39.

Raup, B.H., Kieffer, H.H., Hare, T.M., Kargel, J.S., 2000. Generation of data acquisition requests for the ASTER satellite instrument for monitoring a globally distributed target. Glaciers. IEEE Trans. Geosci. Remote Sens. 38, 1105–1112.

Realmuto, V.J., 1990. Separating the effects of temperature and emissivity: emissivity spectrum normalization. In: Abbott, E.A. (Ed.), Proc. Second Ann. Airborne Earth Sci. Workshop, vol. 90 (55). JPL Publishers, Pasadena, CA, pp. 31–35.

Realmuto, V.J., Abrams, M.J., Buongiorno, M.F., Pieri, D.C., 1994. The use of multispectral thermal infrared image data to estimate the sulfur dioxide flux from volcanoes: a case study from Mount Etna, Sicily, July 29, 1986. J. Geophys. Res. 99, 481–488.

Rothery, D.A., Francis, P.W., Wood, C.A., 1988. Volcano monitoring using short wavelength infrared data from satellites. J. Geophys. Res. 93, 7993–8008.

Salisbury, J.W., D'Aria, D.M., 1992. Emissivity of terrestrial materials in the 8–14 μm atmospheric window. Remote Sens. Environ. 42, 83–106.

Sampson, D.E., 1987. Textural heterogeneities and vent area structures in the 600-year-old lavas of the Inyo volcanic chain, eastern California. In: Fink, J.H. (Ed.), The Emplacement of Silicic Domes and Lava Flows. Spec. Pap. Geol. Soc. Am., 212, 89–101.

Schneider, D.J., Rose, W.I., Coke, L.R., Bluth, G.J.S., Sprod, I.E., Krueger, A.J., 1999. Early evolution of a stratospheric volcanic eruption cloud as observed with TOMS and AVHRR. J. Geophys. Res. 104, 4037–4050.

Schneider, D.J., Dean, K.G., Dehn, J., Miller, T.P., Kirianov, V.Y., 2000. Monitoring and analyses of volcanic activity using remote sensing data at the Alaska Volcano Observatory: case study for Kamchatka, Russia, December 1997. In: Mouginis-Mark, P.J., Crisp, J.A., Fink, J.H. (Eds.), Remote Sensing of Active Volcanism. Monograph. Am. Geophys. Union, Washington, DC, pp. 65–86.

Stefanov, W.L., Ramsey, M.S., Christensen, P.R., 2001. Monitoring the urban environment: an expert system approach to land cover classification of semiarid to arid urban centers. Remote Sens. Environ. 77, 173–185.

Stofan, E.R., Anderson, S.W., Crown, D.A., Plaut, J.J., 2000. Emplacement and composition of steep-sided domes on Venus. J. Geophys. Res. 105, 26757–26771.

Welch, R., Jordan, T., Lang, H., Murakami, H., 1998. ASTER as a source for topographic data in the late 1990's. IEEE Trans. Geosci. Remote Sens. 36, 1282–1289.

Wooster, M.J., Kaneko, T., 1998. Satellite thermal analysis of lava dome effusion rates at Unzen Volcano, Japan. J. Geophys. Res. 103, 20935–20947.

Yamaguchi, Y., Kahle, A., Tsu, H., Kawakami, T., Pniel, M., 1998. Overview of the Advanced Spaceborne Thermal Emission and Reflectance Radiometer (ASTER). IEEE Trans. Geosci. Remote Sens. 36, 1062–1071.